資料 6

Available online at www.sciencedirect.com

SCIENCE DIRECT

Nuclear Medicine and Biology 32 (2005) 21–28

NUCLEAR MEDICINE — AND — BIOLOGY

www.elsevier.com/locate/nucmedbio

Basic characterization of ^{64}Cu-ATSM as a radiotherapy agent

Atsushi Obata[a,b], Shingo Kasamatsu[c], Jason S. Lewis[d], Takako Furukawa[a], Shinji Takamatsu[a], Jun Toyohara[e], Tatsuya Asai[a], Michael J. Welch[d], Susan G. Adams[d], Hideo Saji[b], Yoshiharu Yonekura[a], Yasuhisa Fujibayashi[a,*]

[a]*Biomedical Imaging Research Center, University of Fukui, Matsuoka, Fukui 910-1193, Japan*
[b]*Graduate School of Pharmaceutical Sciences, Kyoto University, Sakyo, Kyoto 606-8151, Japan*
[c]*JFE Fukui Branch, University of Fukui, Matsuoka, Fukui 910-1193, Japan*
[d]*Mallinckrodt Institute of Radiology, Washington University Medical Center, St. Louis, MO 63110, USA*
[e]*Research Center, Research and Development Division, Nihon Medi-Physics, Co. Ltd., Chiba 910-1193, Japan*

Received 24 March 2004; received in revised form 29 July 2004; accepted 20 August 2004

Abstract

^{64}Cu-diacetyl-bis(N^4-methylthiosemicarbazone) (^{64}Cu-ATSM) is a promising radiotherapy agent for the treatment of hypoxic tumors. In an attempt to elucidate the radiobiological basis of ^{64}Cu-ATSM radiotherapy, we have investigated the cellular response patterns in vitro cell line models. Cells were incubated with ^{64}Cu-ATSM, and the dose–response curves were obtained by performing a clonogenic survival assay. Radiation-induced damage in DNA was evaluated using the alkali comet assay and apoptotic cells were detected using Annexin V-FITC and propidium iodide staining methods. Washout rate and subcellular distribution of ^{64}Cu in cells were investigated to further assess the effectiveness of ^{64}Cu-ATSM therapy on a molecular basis. A direct comparison of subcellular localization of Cu-ATSM was made with the flow tracer analog Cu-pyruvladehyde-bis(N^4-methylthiosemicarbazone). In this study, ^{64}Cu-ATSM was shown to reduce the clonogenic survival rate of tumor cells in a dose-dependent manner. Under hypoxic conditions, cells took up ^{64}Cu-ATSM and radioactive ^{64}Cu was highly accumulated in the cells. In the ^{64}Cu-ATSM-treated cells, DNA damage by the radiation emitted from ^{64}Cu was detected, and inhibition of cell proliferation and induction of apoptosis was observed at 24 and 36 h after the treatment. The typical features of postmitotic apoptosis induced by radiation were observed following ^{64}Cu-ATSM treatment. The majority of the ^{64}Cu taken up into the cells remained in the postmitochondrial supernatant (the cellular residue after removal of the nuclei and mitochondria), which indicates that the β^- particle emitted from ^{64}Cu may be as effective as the Auger electrons in ^{64}Cu-ATSM therapy. These data allow us to postulate that ^{64}Cu-ATSM will be able to attack the hypoxic tumor cells directly, as well as potentially affecting the peripheral nonhypoxic regions indirectly by the β^- particle decay of ^{64}Cu.

Keywords: ^{64}Cu-ATSM; Tumor; Internal radiation therapy; Hypoxia; Apoptosis; PET

1. Introduction

Radionuclide therapy is one of the highly promising approaches for treating cancer and is widely investigated in basic research and clinical practice [1]. Radionuclide therapies using labeled antibodies or peptides targeting tumor-related antigens or receptors have been extensively studied especially in the field of hematological malignancies such as lymphoma and leukemia [2–4]. However, success of these agents in solid tumors has been limited mainly due to heterogeneous antigen expression and low overall tumor uptake. A variety of strategies have been employed to improve the tumor targeting and therapy effects of such methods including combination therapy with other modalities [5–8].

Conventionally, low linear energy transfer β-emitters such as ^{131}I, ^{90}Y and ^{186}Re have been widely used for radionuclide therapy [9]. ^{67}Cu also has been investigated as a candidate for radionuclide therapy. ^{67}Cu has excellent physical and biochemical properties for radionuclide therapy and ^{67}Cu-labeled monoclonal antibodies were reported to be useful for the treatment of lymphoma and colorectal carcinoma [9,10]. However, production of ^{67}Cu requires a large accelerator or nuclear reactor, limiting the availability of ^{67}Cu.

* Corresponding author. Tel.: +81 776 61 8430; fax: +81 776 61 8170.
E-mail address: yfuji@fmsrsa.fukui-med.ac.jp (Y. Fujibayashi).

0969-8051/$ – see front matter © 2005 Elsevier Inc. All rights reserved.
doi:10.1016/j.nucmedbio.2004.08.012

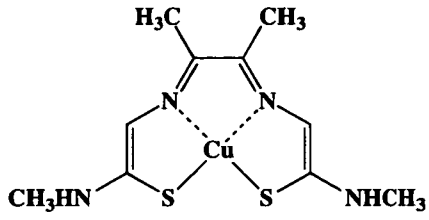

Fig. 1. Structure of Cu-ATSM.

^{64}Cu with a half-life of 12.7 h decays by electron capture (41%), β^- decay (0.573 MeV, 40%) and β^+ decay (0.656 MeV, 19%), accompanied by emission of annihilation radiation (0.511 MeV, 38%) and γ photons (1.34 MeV, 0.5%). It is a promising therapeutic radionuclide because of its favorable β^- particle emissions [11,12]. ^{64}Cu is reported to be as efficient as ^{67}Cu for tumor treatment [13,14] and can be produced using small biomedical cyclotrons in regular PET centers on a daily basis [15,16]. Furthermore, because of its multiple decay modes, ^{64}Cu can be used for real-time PET monitoring of regional drug concentration, kinetics and dosimetry during radiation therapy if it is used to label the therapeutic radiopharmaceuticals.

Copper-diacetyl-bis(N^4-methylthiosemicarbazone) (Cu-ATSM; Fig. 1) has been examined extensively by our group and others as a possible imaging agent to delineate hypoxia within tumors [12,17,18]. Cu-ATSM is taken up into tumor cells rapidly and efficiently and reduced by an enzymatic system of sequential electron transport chains, where monovalent Cu is released from the chelate to be retained subsequently [19]. Considering these characters, ^{64}Cu-ATSM has potential as a radiotherapy agent with an option of real-time PET monitoring. Indeed, as a therapy agent, ^{64}Cu-ATSM was reported to be useful for the treatment of colorectal carcinoma in vivo tumor model [20]. In the present report, we have investigated the molecular basis of ^{64}Cu-ATSM therapy using in vitro tumor cell models. The cell killing ability of ^{64}Cu-ATSM was evaluated by colony-forming assay. Some of the typical features of cell death derived by radiation were observed; namely, inhibition of the cell proliferative rate and apoptotic cell death. Subcellular localization of Cu-ATSM was studied and compared with Cu-pyruvladehyde-bis(N^4-methylthiosemicarbazone) (Cu-PTSM), a flow tracer [21]. We also discuss the fate of ^{64}Cu in relation to cell toxicity. This study may provide useful information for designing effective therapy strategies and improving the radiotherapy efficacy in cancer treatment.

2. Materials and methods

All chemicals were reagent grade. The ^{64}Cu at University of Fukui was produced on a 12-MeV biomedical cyclotron using previously reported methods [15,16]. The ^{64}Cu at Washington University was produced on a CS-15 biomedical cyclotron (Cyclotron) [15]. H_2ATSM was synthesized as described previously [22]. ^{64}Cu-ATSM was prepared by mixing 200 mM glycine buffer containing ^{64}Cu and H_2ATSM in dimethyl sulfoxide (20:1 by volume) [17]. Labeling efficiency was determined by radio-HPLC using conditions described previously [19]. Radiochemical purity and specific activity of ^{64}Cu-ATSM in all studies were >99% and >56,000 GBq/mmol, respectively.

2.1. Cell culture

Mouse Lewis Lung carcinoma LL/2 cells were purchased from Dai-Nippon Seiyaku (Japan) and were grown in a 5% CO_2-humidified atmosphere at 37 °C. Cells were routinely maintained in Dulbecco's modified Eagle Medium (DMEM) (GIBCO, Grand Island, NY) supplemented with 10% fetal bovine serum.

2.2. Uptake of ^{64}Cu-ATSM into cells

Previous reports show that the uptake of ^{64}Cu-ATSM was dramatically increased under hypoxic conditions [23]; therefore, we followed the reported methods during the uptake phase. Briefly, cells were trypsinized and collected in a polypropylene tube (Falcon, Becton Dickinson, Lincoln Park, NJ). Cell numbers were counted with a hemocytometer and the cells were resuspended in serum-free DMEM to a concentration of 1×10^6 cells/ml. Ten million cells were transferred to a three-necked flask and hypoxic gas (95% N_2, 5% CO_2) was passed over the cells at 37 °C for 1.5 h. ^{64}Cu-ATSM was then added to the flask and incubated for 1 h. After incubation, aliquots of the cell suspension were removed and the cells were pelleted from the reaction media to calculate the percentage uptake of ^{64}Cu-ATSM. Additional aliquots of cells were transferred to a polypropylene tube and resuspended with fresh DMEM containing 10% fetal bovine serum for further experiments.

2.3. Clonogenic survival assay

The radiotherapy effect of ^{64}Cu-ATSM was measured by performing a clonogenic survival assay under normoxic condition [24,25] because continuous hypoxia treatment itself affected cell viability. The ^{64}Cu-ATSM-treated cells, resuspended in fresh medium, were counted using a hemocytometer and diluted properly. Cells were seeded into 60-mm dishes (Falcon, Becton Dickinson, Lincoln Park, NJ) and cultured in a humidified 5% CO_2/95% air atmosphere at 37 °C. After 5 days of incubation, the cells were stained with 3% Giemsa solution, and colonies containing more than 50 cells were counted as survivors. The absolute plating efficiencies of control cells were 34.1±9.7%. The surviving fraction was determined as the ratio of live colonies in the ^{64}Cu-ATSM-treated cell populations relative to the glycine-treated control.

2.4. Cell growth assay

After the treatment, cells were seeded in six-well plates (Falcon, Becton Dickinson, Lincoln Park, NJ) and cultured

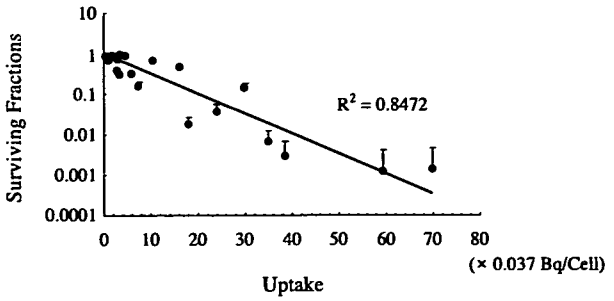

Fig. 2. Clonogenic survival of LL/2 cells treated with ^{64}Cu-ATSM. LL/2 cells were treated with different concentrations of ^{64}Cu-ATSM for 1 h under hypoxic conditions to trap ^{64}Cu metabolically into cells. After the treatment, surplus ^{64}Cu-ATSM was removed and cells were resuspended in fresh culture medium and the radioactivity taken up by the cells was measured. Cells were seeded in 6-cm dishes and cultured for 5 days, and the colonies containing more than 50 cells were counted. The surviving fractions determined as described in Materials and methods was plotted against the amount of ^{64}Cu taken up by the cells. Values are the mean and S.D. ($n=6$).

under normoxic condition. Cells were trypsinized and counted using the trypan blue dye exclusion test at the specified time points.

2.5. Comet assay (single cell gel electrophoresis)

To detect the damage to DNA induced by ^{64}Cu, the comet assay was performed after ^{64}Cu-ATSM treatment [26]. Glycine-treated control cells and ^{64}Cu-ATSM-treated cells were seeded in 100-mm dishes (Falcon, Becton Dickinson) and cultured under normoxic condition. Six hours after the treatment, cells were trypsinized and counted using the trypan blue dye exclusion test. Viability of cells was >90%. The cells were sedimented by centrifugation and adjusted to the concentration of 1×10^5 cells/ml with phosphate-buffered saline. The cells were treated with a

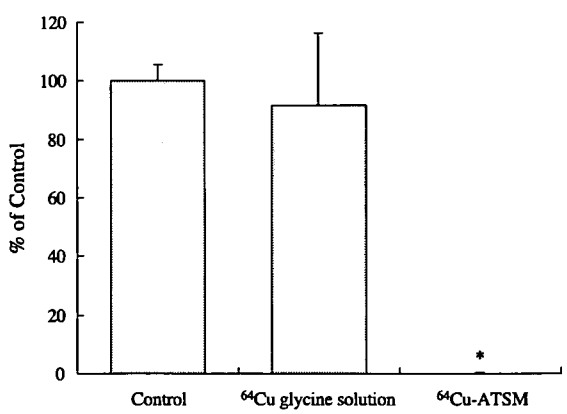

Fig. 3. The effect of carrier-free ^{64}Cu and ^{64}Cu-ATSM on the survival rate of LL/2 cells. A clonogenic survival assay was performed with a control group (treated with glycine solution), a ^{64}Cu-glycine solution-treated group (938.3±41.65 μCi added to 10^7 cells) and a ^{64}Cu-ATSM-treated group (896.7±35.84 μCi added to 10^7 cells). Viability compared with control group was 91.43±24.64% and 0.1247±0.2874%, respectively. *$P<.0001$, significant degrease compared with control (Student's t test, $n=3$).

Table 1
^{64}Cu uptake ratio and radioactivity in tumor cells after 1 h of treatment

	% Uptake	Radioactivity in tumor cells (Bq/cell)
^{64}Cu-glycine	2.47±0.46	0.0857±0.0038
^{64}Cu-ATSM	61.4±17.7	2.04±0.08

Data are expressed as the mean±S.D. ($n=3$).

CometAssay Kit (Trevigen, Gaithersvurg, MD) according to the instruction manual from the manufacturer. After electrophoresis, assay slides were treated with CometAssay Silver Staining Kit (Trevigen) to visualize the assay results. Data analysis was performed using Komet v. 4.0.2 software (Kinetic Imaging, Wirral, UK).

2.6. Measurement of apoptotic cell death

Early stages of apoptosis were identified using an Annexin V-FITC Apoptosis Detection Kit I (Becton Dickinson, San Jose, CA) [27]. After the uptake period, cells were seeded in six-well plates and cultured under normoxic condition. At the specified time points, cells were collected and stained with Annexin V-FITC/propidium iodide (PI) according to the manufacturer's protocol. Level of apoptosis was quantified using a Becton Dickinson FACSCalibur system and analyzed using CellQuest v. 3.1 software (Becton Dickinson, San Jose, CA). Cells that were Annexin

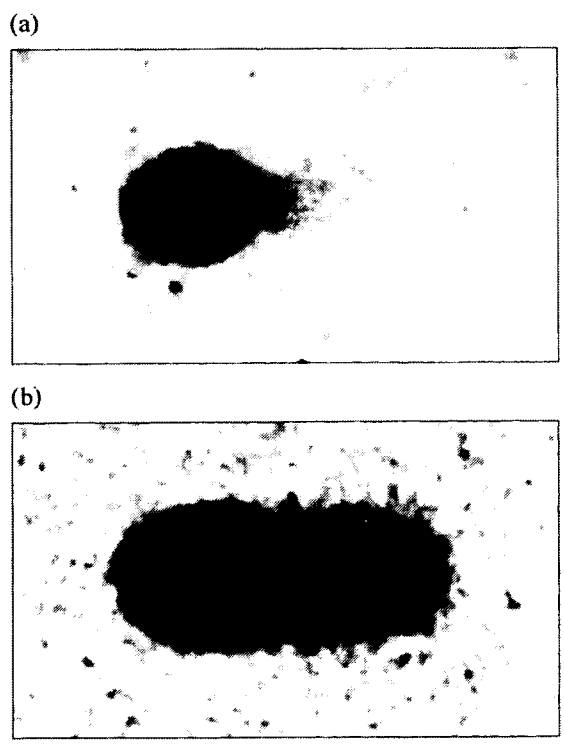

Fig. 4. The typical microscopic images following the comet assay at 6 h after treatment. Images of a normal cell (a) and DNA-damaged cell (b) are shown. In the ^{64}Cu-ATSM-treated groups, over 90% of total cells suffered from DNA damage and displayed damaged pattern as shown in b.

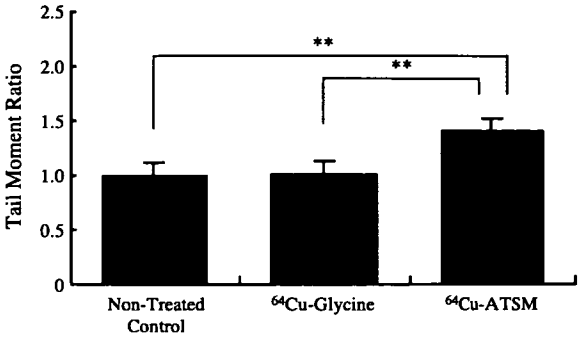

Fig. 5. Tail moment ratio in the comet assay. Forty cells were selected ad libitum and then analyzed for the tail moment using the Comet v. 4.0.2 software. Data are presented as a ratio to the nontreated control groups (bar, 1 S.E.). $^{**}P<.01$, significant increase (Student's t test).

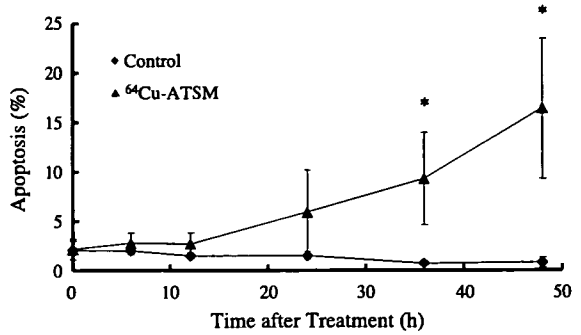

Fig. 7. Apoptosis of LL/2 cells after ^{64}Cu-ATSM treatment. Floating and adherent cells were collected, stained with Annexin V-FITC and PI, then analyzed by FACS using CellQuest software. A significant increase in apoptosis was observed with ^{64}Cu-ATSM-treated cells from 36 h after the treatment. Data points are the average percentage of apoptotic cells and S.D. ($n=3$). $^{*}P<.05$, significant increase (Student's t test).

V-FITC-positive and PI-negative were identified as apoptotic cells as described previously [28,29].

2.7. Retention and intracellular distribution of ^{64}Cu-ATSM and ^{64}Cu-PTSM in LL/2 cells

Cells were incubated in hypoxic gas (95% N_2, 5% CO_2) for 1.5 h at which point either ^{64}Cu-ATSM or ^{64}Cu-PTSM was added to the media. Following a 1-h incubation, the media was removed and the cells in fresh medium were seeded in 100-mm dishes, cultured under normoxic condition and recollected at 0, 1, 3, 6, 12 and 24 h after the treatment. Cells were washed twice with an ice-cold isolation medium (0.25 M sucrose buffered to pH 7.4 with 10 mM HEPES). Aliquots of cells were separated and the radioactivity in the cells was counted using a γ-counter (ARC-2000, ALOKA, Japan). Another aliquot of the cells was resuspended in ice-cold lysis buffer (0.005% SDS buffered to pH 7.4 with 10 mM HEPES) and homogenized. After homogenization, the P1 fraction (crude nuclear fraction) was obtained by centrifugation at 1000×g for 5 min at 4 °C. The supernatant was centrifuged at 8000×g for 10 min at 4 °C to yield the P2 (crude mitochondrial) and S2 (the postmitochondrial supernatant which contains the cellular residue after removal of the nuclei and mitochondria) fraction. Radioactivity in each fraction was measured.

3. Results

Fig. 2 shows the radiation dose–response curve for the LL/2 cells treated with ^{64}Cu-ATSM. Clonogenic survival was decreased in a dose-dependent manner. ^{64}Cu-ATSM uptake of 1.50 Bq/cell produced 99% killing of the cells. Mock treatment with H_2ATSM or nonradioactive Cu-ATSM did not affect the survival ratio of LL/2 cells (data not shown), which also indicates that hypoxia treatment during uptake phase did not affect the cell viability by itself.

The effect of "free" ^{64}Cu ion and ^{64}Cu-ATSM on tumor cells was also compared using the clonogenic survival assay. When approximately 34.8 MBq of ^{64}Cu-glycine solution was inoculated, the survival rate of cells was not affected, whereas the equivalent amount of ^{64}Cu-ATSM treatment produced nearly complete killing of LL/2 cells (Fig. 3). The ^{64}Cu uptake ratio in each treatment was 2.47±0.459% and 61.4±17.7%, respectively, which means the radioactivity

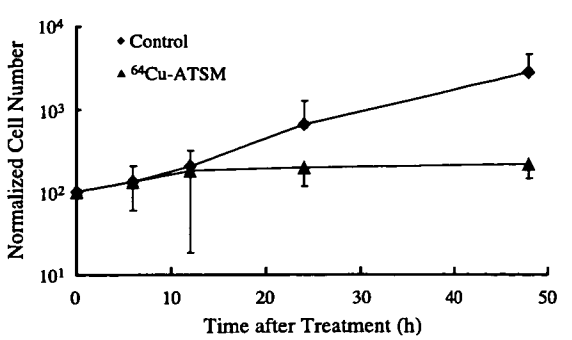

Fig. 6. Growth curve of LL/2 cells after ^{64}Cu-ATSM treatment. Proliferation of the cells was inhibited 24 h after the treatment. Data are presented as normalized cell number ± S.D. relative to time 0 ($n=3$).

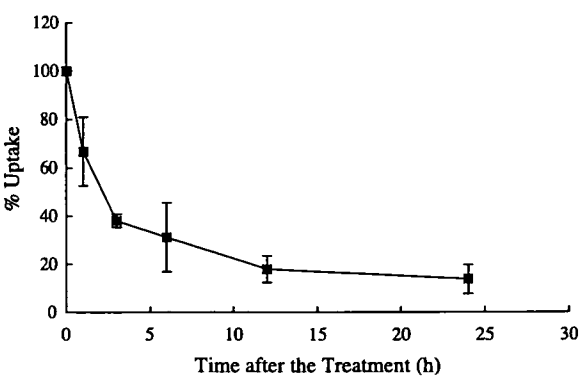

Fig. 8. Washout rate of ^{64}Cu from LL/2 cells; 1×10^7 cells were treated with ^{64}Cu-ATSM and radioactivity in the cell fractions was measured at each time point. Data are shown as ratio to the initial radioactivity after the decay correction. Each data point is the average ± S.D. ($n=3$).

taken up into tumor cells was 0.0857 ± 0.0038 and 2.04 ± 0.08 Bq/cell, respectively. The result suggests that intracellular uptake is the major factor in the efficient tumor cell killing by ^{64}Cu-ATSM (Table 1).

To elucidate the mechanism of cell killing by ^{64}Cu-ATSM, the comet assay was performed 6 h after the ^{64}Cu-ATSM treatment. Fig. 4 shows a typical microscopic image of the results. In the ^{64}Cu-ATSM-treated groups, over 90% of the total cells showed comet tails. The tail moment ratio was significantly increased in the ^{64}Cu-ATSM-treated groups compared with ^{64}Cu-glycine and nontreated control groups (Fig. 5) (nontreated group, P=.0085; ^{64}Cu-glycine-treated group, P=.0085). These results indicated that the radiation emitted from the intracellular ^{64}Cu caused DNA strand breaks, with the maximum recoil energy from the transmutation of ^{64}Cu to its highly charged daughter nucleus potentially increasing the cell killing ability. This damage in the DNA is thought to be one of the major triggers of cell death pathways. Fig. 6 shows the proliferation rate of LL/2 cells after the treatment. In the ^{64}Cu-ATSM-treated group, cell proliferation was completely inhibited after 24 h and a significant apoptotic fraction was seen 36 h after the treatment (P<.05) (Fig. 7).

Both the washout rate and subcellular distribution of ^{64}Cu were investigated in this study. Also, a direct comparison of the subcellular localization was made between ^{64}Cu-ATSM and ^{64}Cu-PTSM. With ^{64}Cu-ATSM, defining the amount of radioactivity associated with the cells at the time of resuspension as 100%, 38.0% of the radioactivity remained at 3 h posttreatment and 31.2% at 6 h posttreatment (Fig. 8). Considering the half-life of ^{64}Cu, the effect of radiation emitted from ^{64}Cu up to 12 h after treatment dominates in this study: about 14,200 decays occurred in one cell up to 12 h after treatment (Fig. 9). In the subcellular fractionation comparison, the distribution of ^{64}Cu from both ^{64}Cu-ATSM and ^{64}Cu-PTSM was very similar (Fig 10). For both ^{64}Cu-ATSM and ^{64}Cu-PTSM, the majority of the radioactivity remained in the S2 fraction over the 24 h. A transition of the radioactivity from the S2 and mitochondria fraction to the nuclear fraction was noted over the 24-h period (Fig. 10).

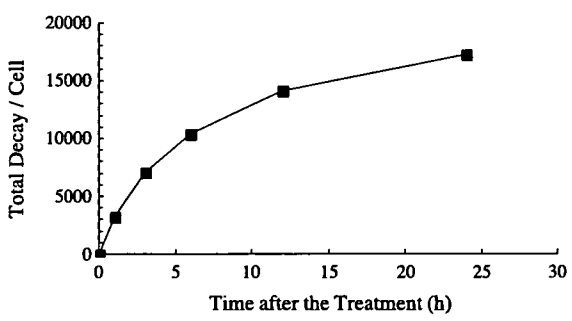

Fig. 9. Total decay frequency of intracellular ^{64}Cu. Based on the washout result shown in Fig. 8, the total decay frequency was calculated for a cell taking up a 99% cell killing dose of 1.50 Bq/cell. Radioactivity at each time point was corrected for a half-life of 12.7 h and the area under the curve was calculated.

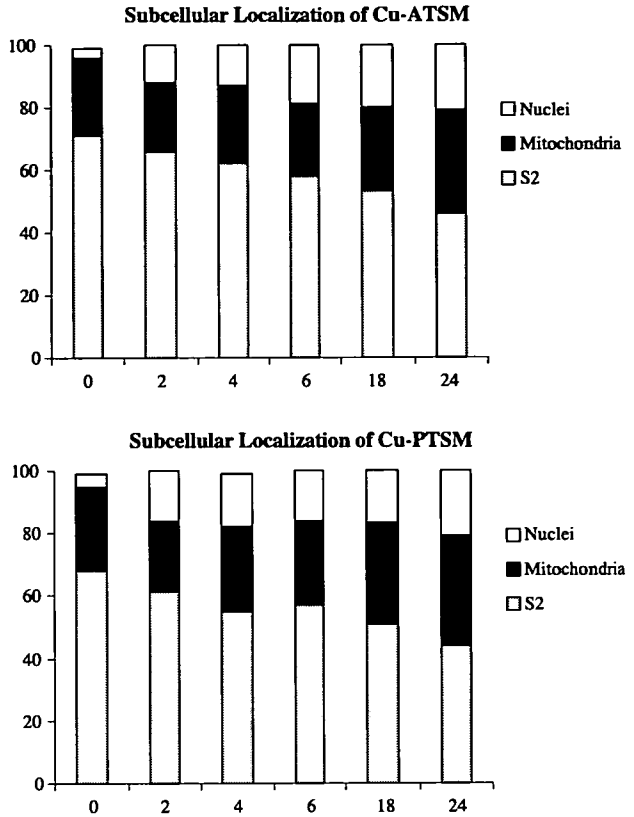

Fig. 10. Subcellular distribution of ^{64}Cu following ^{64}Cu-ATSM or ^{64}Cu-PTSM treatment. After ^{64}Cu-ATSM and ^{64}Cu-PTSM were metabolized in the cells, the majority of the ^{64}Cu was retained in the microsomal/cytosol fraction. A transition of radioactivity from the mitochondria and S2 fractions to the nuclear fractions was noted. Data are expressed as the mean percentage of total cellular radioactivity (n=4).

4. Discussion

^{64}Cu-ATSM has distinct accumulation mechanisms that are based on hypoxic tumor-selective metabolism by some enzymes [19]. Equipped with the radionuclidic characteristics of ^{64}Cu and the high and specific accumulation in tumor cells, ^{64}Cu-ATSM is making a new type of radiotherapy agent that provides a new strategy for the treatment of tumors [20]. In this study, we investigated the cytotoxic effect of ^{64}Cu-ATSM using clonogenic survival assays in an in vitro cell culture model. ^{64}Cu-ATSM decreased the clonogenic survival of LL/2 cells in a dose-dependent manner where 99% cell killing occurred when 1.50 Bq/cell of ^{64}Cu was taken up into the cells.

The nonligand binding form of ^{64}Cu (Cu-glycine) did not affect the survival rate of LL/2 cells, whereas the equivalent amount of radioactivity of ^{64}Cu-ATSM significantly reduced the survival rate to about 0.1% (P<.0001). In this experiment, the incubation medium containing ^{64}Cu was exchanged into fresh culture medium after the treatment,

meaning that the ^{64}Cu taken up into tumor cells prior to the exchange was the only source of the cell killing. The ^{64}Cu taken up into the cells was dramatically different between the ^{64}Cu-glycine-treated groups and the ^{64}Cu-ATSM-treated groups, 0.0857±0.0038 and 2.04±0.08 Bq/cell, respectively. This may be the major cause for the differences in the subsequent survival rates. Furthermore, considering that there was no difference in the survival rate between the nontreated control and ^{64}Cu-glycine groups, the radioactive emissions from outside of the cells during the 1-h treatment in the flask did not affect the tumor cell survival. To be brief, the most effective character of ^{64}Cu-ATSM is to accumulate radioactive ^{64}Cu into the cells and as such produces the ability to kill tumor cells.

Radiation causes direct and/or indirect effects on irradiated cells. One of the well-known direct effects is damage to DNA. DNA damage by ionizing radiation predominantly consists of single-strand breaks, but also includes double-strand breaks, alkali-label sites, and oxidized purines and pyrimidines [30–32]. We confirmed with the alkali comet assay that a significant increase in DNA damage was observed with ^{64}Cu-ATSM-treated groups at 6 h after treatment. Comet assay allows us to detect the DNA fragmentation in apoptotic and/or necrotic cells [33]. However, we could not detect significant increases in the number of apoptotic cells as well as necrotic and/or dead cells using the Annexin V-FITC/PI staining method at the same time point. For this reason, the DNA damage observed after the treatment was considered to be caused directly by the radiation from intracellular ^{64}Cu and not by apoptosis.

Radiation-induced DNA damage elicits a variety of cellular responses including apoptosis as one of the major mechanisms of cell death in radiation therapy [34–36]. In this study, apoptosis marker-positive cells significantly increased in number ($P<.05$) 36 h after the treatment when detected by the Annexin V-FITC/PI staining method, preceded by the inhibition of cellular proliferation 24 h after the treatment. In an X-irradiation study, high-dose irradiation was reported to induce a rapid and strong apoptotic response, whereas low-dose irradiation induced a slow and mild apoptosis; each type of apoptosis was defined as premitotic apoptosis and postmitotic apoptosis, respectively [37]. In the postmitotic apoptosis, cell death occurs after one or a few cell divisions, not immediately after the radiation, and cell cycle arrest is observed at the G_2/M phase. In our preliminary study, we also observed increase of G_2/M phase cells, namely, G_2/M arrest, in the ^{64}Cu-ATSM-treated groups at 12–24 h after the treatment. These findings indicated that the typical cell death after ^{64}Cu-ATSM treatments is through postmitotic apoptosis.

It is conceivable that ^{64}Cu-ATSM would be able to exert stronger cytotoxicity via premitotic apoptosis if a higher radiation dose of ^{64}Cu-ATSM was given to the cells. However, considering radiotherapy in clinical setting, doses should be reduced to avoid adverse effects on nontarget tissues. In this regard, the ability of ^{64}Cu-ATSM to induce mild but steady cytotoxicity and postmitotic apoptosis confirmed in this study is desirable as a radiotherapy agent.

Recently, it has been reported that the damage to DNA by ^{64}Cu might be derived from Auger electrons because about 40% of ^{64}Cu decays by electron capture emitting Auger electrons with high linear electron transfer [20]. Auger electrons are expected to bring very high toxicity if they are in close proximity to DNA. The tissue penetration range of Auger electrons emitted from ^{64}Cu is about 5 μm [20] and is shorter than the diameter of most tumor cells, so it is well recognized that the radiotoxicity of Auger electron emitters depends strongly on their distribution within the cell. The most severe effects have been observed when the Auger emitter is localized in the nucleus [38]. Therefore, also in the case of ^{64}Cu, it is necessary for the radiocopper to localize in the nucleus and around the DNA to exert cytotoxicity through Auger electrons. In this study, we investigated the subcellular distribution of ^{64}Cu after uptake into tumor cells and showed that the radioactivity existed mainly in the S2 fraction with the radioactivity slowly migrating into the nucleus over time. Furthermore, nonradioactive Cu-ATSM did not affect the survival rate, which indicated the Cu ions themselves were not cytotoxic at the concentrations used in this study. Based on these findings, β^- particles emitted from intracellular ^{64}Cu as well as the Auger emissions of ^{64}Cu in the nuclear fraction are considered to be the major cytotoxic sources in ^{64}Cu-ATSM therapies. Moreover, the maximum recoil energy from the transmutation of ^{64}Cu to its highly charged daughter nucleus may also increase the cell killing ability. The multiplicity of decay mode of ^{64}Cu seems to be working in favor of the antitumor effect of ^{64}Cu-ATSM. Previous reports showed a significant portion of ^{67}Cu-pyruvaldehyde-bis(N^4-methylthiosemicarbazone), an analog of the series of Cu(II)-bis(thiosemicarbazones) compounds, is delivered to the cell nucleus [21] and our current studies have demonstrated similar uptake patterns.

The tissue penetration range of β^- particles emitted from ^{64}Cu is up to several hundred of micrometers. For this reason, the cytotoxic effect of the β^- particle of ^{64}Cu can range not only to the single cell that take up ^{64}Cu but also to the surrounding cells that do not take up ^{64}Cu, which could increase the antitumor effect in vivo ^{64}Cu-ATSM therapy. This feature becomes important when treating in vivo tumor masses because aggregation of the cells with heterogeneous characters is expected in vivo tumors.

The washout rate of ^{64}Cu from tumor cells is relatively high in our experimental model. At 3 h after the treatment, radioactivity in the cells was reduced to 38.0% of the total uptake at the end of the treatment. However, in the biodistribution study using tumor-bearing animal models, accumulation of ^{64}Cu-ATSM into tumor cells was reported to be highest at 4 h after injection [20]. High washout rate observed in our assay system might be limited only to in vitro model and actual accumulation of ^{64}Cu in the tumor might continue for much longer periods. If so, the

therapeutic effectiveness of ^{64}Cu-ATSM might be higher in the in vivo tumors.

Based on the washout rate and half-life of ^{64}Cu, we calculated the total number of atomic disintegrations of ^{64}Cu occurring in the tumor cells when 1.50 Bq/cell of ^{64}Cu, a 99% cell killing dose, was taken up into cells (Fig. 9). Under these conditions, approximately 10,000 atomic disintegrations occurred within 6 h after the treatment, and about 14,000 within 12 h. That is, 10,000–14,000 atomic disintegrations per cell might be enough for killing tumor cells. D37 value (37% cell death) [39] was ca. 4500 decay per cell when biological washout from the cells was taken into account for the calculation, which was one fourth of the value previously reported (16,000 decay per cell) [40]. The actual area under time–radioactivity curve in the present study (Fig. 8) was about one fourth of the estimated value from nonwashout model, so that the present result is considered to be more accurate as actual retention pattern was included into the calculation.

In this study, the cells were kept under hypoxic condition during uptake phase of ^{64}Cu-ATSM to realize high retention of ^{64}Cu for 1 h, then cultured for 5 days at the maximum in normoxic condition to evaluate solely the effect of radiation, excluding the effect of hypoxia on cell viability. As hypoxia is considered to lessen the radiation toxicity in general, the cell killing ability determined in this study in normoxic tumor cells might be higher than that expected in continuously hypoxic tumor cells. On the other hand, the present results can be used for the estimation of cell toxicity in normoxic nontumor cells. Hypoxia selectivity of ^{64}Cu-ATSM is critical for realizing tumor-selective treatment. In our human studies using ^{62}Cu-ATSM, the highest accumulation was found in lung tumor (tumor/blood=3.00±1.50), followed by liver (liver/blood=2.45±1.03), whereas other normal tissues showed relatively low accumulation (heart/blood=1.84±0.35, lung/blood=0.43±0.09) [41]. High abdominal accumulation observed in mice [23] might be a result of hepatobiliary secretion of ^{64}Cu after metabolism. From these findings, cytotoxicity in the liver and, to a lesser extent, in the intestine arise as a possible problem in ^{64}Cu-ATSM treatment. Roughly 75% of the blood entering the liver is from portal vein and 25% from hepatic artery. Thus, considerable part of the liver seems to be hypoxic and it might be responsible for the rather high uptake of ^{64}Cu-ATSM in the liver. If so, radiation effect of ^{64}Cu in the liver could be estimated in a similar manner as in hypoxic tumor cells. Physiological excretion route of Cu is from liver to duodenum. Radioactive ^{64}Cu injected as Cu-ATSM is also expected to follow this route after released from the chelate. As shown in the present study, extracellular ^{64}Cu did not show significant cell toxicity, so that radioactivity in the duodenum is less likely to become a source of adverse effect in the treatment.

In vitro cell uptake study reported previously, Cu-ATSM showed some uptake also in normoxic tumor cells [23]. However, in our PET studies in normal human, selective Cu accumulation was found only in the liver but no other tissues (unpublished data). Thus, the uptake in the normoxic tumor cells might be from a characteristic of tumor cells. In fact, tumor cells expressed microsomal electron transport enzymes and they played a major role in reductive retention of Cu-ATSM in tumor cells, especially under hypoxic conditions [19]. Thus, Cu-ATSM can be evaluated mainly as a marker of hypoxia and, in some part, as a marker of tumor-selective gene expression by means of microsomal enzyme expression, in clinical practice.

5. Conclusion

^{64}Cu-ATSM has been shown to be effective in the treatment of tumors. ^{64}Cu-ATSM efficiently delivered radioactive ^{64}Cu into hypoxic tumor cells and the emitted β^- particles caused lethal damage to DNA leading to postmitotic apoptosis and mild but steady cell death. Since Cu-ATSM showed low but considerable uptake in normoxic cells in vitro and may be taken up in normoxic cells in vivo, the therapeutic index need to be carefully considered. In order to ensure the safety and effectiveness of ^{64}Cu-ATSM treatment, contribution of hypoxia on both ^{64}Cu accumulation and radiation sensitivity of target and/or nontarget cells and possible adverse effects to the excretion route should be clarified.

Acknowledgments

Part of this study is supported by a Grant-in-Aid for Scientific Research (Kakenhi No. 1430274) from JSPS, Research and Development Project Aimed at Economic Revitalization from the Ministery of Education, Culture, Science, Sports and Technology Japan, and the 21st Century COE program "Biomedical Imaging Technology Integration Program" from JSPS.

The production of Cu-64 at Washington University is supported by NCI R24 CA86307. Additional financial support for the studies at Washington University came from the United States Department of Energy grant (DE-FG02-87ER60212).

References

[1] Zuckier LS, DeNardo GL. Trials and tribulations: oncological antibody imaging comes to the fore. Semin Nucl Med 1997;27(1): 10–29.

[2] Burke JM, Jurcic JG, Scheinberg DA. Radioimmunotherapy for acute leukemia. Cancer Control 2002;9(2):106–13.

[3] Frankel AE, Sievers EL, Scheinberg DA. Cell surface receptor-targeted therapy of acute myeloid leukemia: a review. Cancer Biother Radiopharm 2000;15(5):459–76.

[4] Postema EJ, Boerman OC, Oyen WJ, Raemaekers JM, Corstens FH. Radioimmunotherapy of B-cell non-Hodgkin's lymphoma. Eur J Nucl Med 2001;28(11):1725–35.

[5] Burke PA, DeNardo SJ, Miers LA, Kukis DL, DeNardo GL. Combined modality radioimmunotherapy. Promise and peril. Cancer 2002;94(4 Suppl):1320–31.

[6] Choy H, Akerley W, Glantz M, Safran H, Graziano S, Chung C. Concurrent paclitaxel and radiation therapy for solid tumors. Cancer Control 1996;3(4):310–8.
[7] Colcher D, Bird R, Roselli M, Hardman KD, Johnson S, Pope S, et al. In vivo tumor targeting of a recombinant single-chain antigen-binding protein. J Natl Cancer Inst 1990;82(14):1191–7.
[8] Smyth MJ, Pietersz GA, McKenzie IF. Use of vasoactive agents to increase tumor perfusion and the antitumor efficacy of drug-monoclonal antibody conjugates. J Natl Cancer Inst 1987;79(6):1367–73.
[9] Delaloye AB, Delaloye B, Buchegger F, Vogel CA, Gillet M, Mach JP, et al. Comparison of copper-67- and iodine-125-labeled anti-CEA monoclonal antibody biodistribution in patients with colorectal tumors. J Nucl Med 1997;38(6):847–53.
[10] Kroger LA, DeNardo GL, Gumerlock PH, Xiong CY, Winthrop MD, Shi XB, et al. Apoptosis-related gene and protein expression in human lymphoma xenografts (Raji) after low dose rate radiation using ^{67}Cu-2IT-BAT-Lym-1 radioimmunotherapy. Cancer Biother Radiopharm 2001;16(3):213–25.
[11] Anderson CJ, Schwarz SW, Connett JM, Cutler PD, Guo LW, Germain CJ, et al. Preparation, biodistribution and dosimetry of copper-64-labeled anti-colorectal carcinoma monoclonal antibody fragments 1A3-F(ab′)2. J Nucl Med 1995;36(5):850–8.
[12] Lewis JS, Lewis MR, Cutler PD, Srinivasan A, Schmidt MA, Schwarz SW, et al. Radiotherapy and dosimetry of ^{64}Cu-TETA-Tyr3-octreotate in a somatostatin receptor-positive, tumor-bearing rat model. Clin Cancer Res 1999;5(11):3608–16.
[13] Apelgot S, Coppey J, Gaudemer A, Grisvard J, Guille E, Sasaki I, et al. Similar lethal effect in mammalian cells for two radioisotopes of copper with different decay schemes, ^{64}Cu and ^{67}Cu. Int J Radiat Biol 1989;55(3):365–84.
[14] Connett JM, Anderson CJ, Guo LW, Schwarz SW, Zinn KR, Rogers BE, et al. Radioimmunotherapy with a ^{64}Cu-labeled monoclonal antibody: a comparison with ^{67}Cu. Proc Natl Acad Sci U S A 1996; 93(13):6814–8.
[15] McCarthy DW, Shefer RE, Klinkowstein RE, Bass LA, Margeneau WH, Cutler CS, et al. Efficient production of high specific activity ^{64}Cu using a biomedical cyclotron. Nucl Med Biol 1997;24(1):35–43.
[16] Obata A, Kasamatsu S, McCarthy DW, Welch MJ, Saji H, Yonekura Y, et al. Production of therapeutic quantities of ^{64}Cu using a 12 MeV cyclotron. Nucl Med Biol 2003;30(5):535–9.
[17] Fujibayashi Y, Cutler CS, Anderson CJ, McCarthy DW, Jones LA, Sharp T, et al. Comparative studies of Cu-64-ATSM and C-11-acetate in an acute myocardial infarction model: ex vivo imaging of hypoxia in rats. Nucl Med Biol 1999;26(1):117–21.
[18] Fujibayashi Y, Taniuchi H, Yonekura Y, Ohtani H, Konishi J, Yokoyama A. Copper-62-ATSM: a new hypoxia imaging agent with high membrane permeability and low redox potential. J Nucl Med 1997;38(7):1155–60.
[19] Obata A, Yoshimi E, Waki A, Lewis JS, Oyama N, Welch MJ, et al. Retention mechanism of hypoxia selective nuclear imaging/radiotherapeutic agent Cu-diacetyl-bis(N^4-methylthiosemicarbazone) (Cu-ATSM) in tumor cells. Ann Nucl Med 2001;15(6):499–504.
[20] Lewis J, Laforest R, Buettner T, Song S, Fujibayashi Y, Connett J, et al. Copper-64-diacetyl-bis(N^4-methylthiosemicarbazone): an agent for radiotherapy. Proc Natl Acad Sci U S A 2001;98(3):1206–11.
[21] Baerga ID, Maickel RP, Green MA. Subcellular distribution of tissue radiocopper following intravenous administration of ^{67}Cu-labeled Cu-PTSM. Int J Radiat Appl Instrum B 1992;19(6):697–701.
[22] Gingras BA, Suprunchuk T, Bayley CH. The preparation of some thiosemicarbazones and their copper complexes. Can J Chem 1962; 40:1053–9.
[23] Lewis JS, McCarthy DW, McCarthy TJ, Fujibayashi Y, Welch MJ. Evaluation of ^{64}Cu-ATSM in vitro and in vivo in a hypoxic tumor model. J Nucl Med 1999;40(1):177–83.
[24] Rao GS, Murray S, Ethier SP. Radiosensitization of human breast cancer cells by a novel ErbB family receptor tyrosine kinase inhibitor. Int J Radiat Oncol Biol Phys 2000;48(5):1519–28.
[25] Rockwell S. In vivo–in vitro tumor systems: new models for studying the response of tumors to therapy. Lab Anim Sci 1977;27:813–51.
[26] Rojas E, Lopez MC, Valverde M. Single cell gel electrophoresis assay: methodology and applications. J Chromatogr, B Biomed Sci Appl 1999;722:225–54.
[27] Swart JM, Chiles TC. Rescue of CH31 B cells from antigen receptor-induced apoptosis by inhibition of p38 MAPK. Biochem Biophys Res Commun 2000;276(2):417–21.
[28] Hertveldt K, Philippe J, Thierens H, Cornelissen M, Vral A, De Ridder L. Flow cytometry as a quantitative and sensitive method to evaluate low dose radiation induced apoptosis in vitro in human peripheral blood lymphocytes. Int J Radiat Biol 1997;71(4):429–33.
[29] Vermes I, Haanen C, Steffens-Nakken H, Reutelingsperger C. A novel assay for apoptosis. Flow cytometric detection of phosphatidylserine expression on early apoptotic cells using fluorescein labelled Annexin V. J Immunol Methods 1995;184(1):39–51.
[30] Frankenberg-Schwager M. Induction, repair and biological relevance of radiation-induced DNA legions in eukaryotic cells. Radiat Environ Biophys 1990;29:273–92.
[31] Goodhead DT. Initial events in the cellular effects of ionizing radiations: clustered damage in DNA. Int J Radiat Biol 1994;65(1): 7–17.
[32] Ward JF. Radiation mutagenesis: the initial DNA lesions responsible. Radiat Res 1995;142(3):362–8.
[33] Godard T, Deslandes E, Lebailly P, Vigreux C, Sichel F, Poul JM, et al. Early detection of staurosporine-induced apoptosis by comet and annexin V assays. Histochem Cell Biol 1999;112(2):155–61.
[34] Knox SJ, Sutherland W, Goris ML. Correlation of tumor sensitivity to low-dose-rate irradiation with G2/M-phase block and other radiobiological parameters. Radiat Res 1993;135(1):24–31.
[35] Kroger LA, DeNardo SJ, DeNardo GL, Xiong CY, Winthrop MD, Gumerlock PH. Effect of ^{67}Cu-2IT-BAT-Lym-1 therapy on BCL-2 gene and protein expression in a lymphoma mouse model. Clin Cancer Res 1999;5(10 Suppl):3010s–4s.
[36] Macklis RM, Beresford BA, Palayoor S, Sweeney S, Humm JL. Cell cycle alterations, apoptosis, and response to low-dose-rate radioimmunotherapy in lymphoma cells. Int J Radiat Oncol Biol Phys 1993;27(3):643–50.
[37] Shinomiya N, Kuno Y, Yamamoto F, Fukasawa M, Okumura A, Uefuji M, et al. Different mechanisms between premitotic apoptosis and postmitotic apoptosis in X-irradiated U937 cells. Int J Radiat Oncol Biol Phys 2000;47(3):767–77.
[38] Hofer KG, Harris CR, Smith M. Radiotoxicity of intracellular Ga-67, I-125 and H-3. Nuclear versus cytoplasmic radiation effects in murine L1210 leukaemia. Int J Radiat Biol Relat Stud Phys Chem Med 1975;28:225–41.
[39] Hall EJ. The shape of the survival curve. In: Hall EJ, editor. Radiobiology for the radiologist. Philadelphia: J.B. Lippincott Co; 1994. p. 32–9.
[40] Anderson CJ, Connett JM, Baumann ML, Schwarz SW, Zinn KR, Phlipott GW, et al. Comparison of Cu-67 and Cu-64 as potential radionuclides for radiotherapy. J Nucl Med 1993;34(5):134P.
[41] Takahashi N, Fujibayashi Y, Yonekura Y, Welch MJ, Waki A, Tsuchida T, et al. Evaluation of ^{62}Cu labeled diacetyl-bis(N^4-methylthiosemicarbazone) as a hypoxic tissue tracer in patients with lung cancer. Ann Nucl Med 2000;14(5):323–8.

資料(7)

Available online at www.sciencedirect.com

SCIENCE DIRECT

Nuclear Medicine and Biology 33 (2006) 281–286

NUCLEAR MEDICINE — AND — BIOLOGY

www.elsevier.com/locate/nucmedbio

Automatic synthesis of 16α-[^{18}F]fluoro-17β-estradiol using a cassette-type [^{18}F]fluorodeoxyglucose synthesizer

Tetsuya Mori[a,*], Shingo Kasamatsu[b], Christoph Mosdzianowski[c], Michael J. Welch[d], Yoshiharu Yonekura[a], Yasuhisa Fujibayashi[a]

[a]*Biomedical Imaging Research Center, University of Fukui, Matsuoka, Fukui 910-1193, Japan*
[b]*JFE P&S Fukui Branch, University of Fukui, Matsuoka, Fukui 910-1193, Japan*
[c]*GE Healthcare Technologies, Parc Scientifique du Sart Tilman Av. Pre-Aliy (c/o Socran) B-4031 Lieage, Belgium*
[d]*Mallinckrodt Institute of Radiology, Washington University Medical Center, St. Louis, MO 63110, USA*

Received 22 March 2005; received in revised form 2 November 2005; accepted 6 November 2005

Abstract

16α-[^{18}F]fluoro-17β-estradiol ([^{18}F]FES) is a radiotracer for imaging estrogen receptors by positron emission tomography. We developed a clinically applicable automatic preparation system for [^{18}F]FES by modifying a cassette-type [^{18}F]fluorodeoxyglucose synthesizer. Two milligrams of 3-*O*-methoxymethyl-16,17-*O*-sulfuryl-16-epiestriol in acetonitrile was heated at 105°C for 10 min with dried [^{18}F]fluoride. The resultant solution was evaporated and hydrolyzed with 0.2 N HCl in 90% acetonitrile/water at 95°C for 10 min under pressurized condition. The neutralization was carried out with 2.8% $NaHCO_3$, and then the high-performance liquid chromatography (HPLC) purification was performed. The desired radioactive fraction was collected and the solvent was replaced by 10 ml of saline, and then passed through a 0.22-μm filter into a pyrogen-free vial as the final product. The HPLC purification data demonstrated that [^{18}F]FES was synthesized with a yield of 76.4±1.9% (n=5). The yield as the final product for clinical use was 42.4±3.2% (n=5, decay corrected). The total preparation time was 88.2±6.4 min, including the HPLC purification and the solvent replacement process. The radiochemical purity of the final product was >99%, and the specific activity was more than 111 GBq/μmol. The final product was stable for more than 6 h in saline containing sodium ascorbate. This new preparation system enables us to produce [^{18}F]FES safe for clinical use with high and reproducible yield.

Keywords: [^{18}F]FES; Estrogen receptors; Automatic synthesis; Radiopharmaceutical; PET; Cassette-type FDG synthesizer

1. Introduction

The estrogen receptor (ER) status is an important prognostic factor in breast cancer because the ER positive cancers are less aggressive in clinical course and likely to respond to hormonal therapy [1]. The ER expression can be estimated with biopsied material; however, sampling errors may occur when patients have large or multisite tumors. 16α-[^{18}F]fluoro-17β-estradiol ([^{18}F]FES) has been developed as a tracer for imaging ER by positron emission tomography (PET) [2,3]. In clinical studies, the uptakes of [^{18}F]FES were proportional to the ER concentration in both primary and metastatic breast cancers [4–7]. FES-PET information may predict the response of the advanced breast cancer to hormonal therapy and may be useful for guiding better treatment. Therefore, [^{18}F]FES is one of the most promising radiopharmaceutical for monitoring of ER status in breast cancer; however, it is not widely used because of the difficulty of the synthesis. The first synthesis of [^{18}F]FES was reported by Kiesewetter et al. [8], and the application of robotic synthesis was evolved [9]. Their procedure involved reduction by $LiAlH_4$ and liquid N_2. Another procedure was reported, which uses 3-*O*-methoxymethyl-16,17-*O*-sulfuryl-16-epiestriol (**1**) as a precursor [10,11]. The advantages of the latter procedure are that the nucleophilic substitution by [^{18}F]fluoride proceeded rapidly with good yield, and this precursor is commercially available. It is also advantageous that the hydrolysis reactions were performed under mild condition [12]. Although the automatic synthesis of [^{18}F]FES using

* Corresponding author. Tel.: +81 776 61 8491; fax: +81 776 61 8170.
E-mail address: morit@fmsrsa.fukui-med.ac.jp (T. Mori).

0969-8051/$ – see front matter © 2006 Published by Elsevier Inc.
doi:10.1016/j.nucmedbio.2005.11.002

[^{18}F]fluorodeoxyglucose (FDG) synthesis module was reported [13], reproducible yield of [^{18}F]FES could not be realized because of the complex reaction conditions and purification processes.

[^{18}F]fluorodeoxyglucose synthesis has become a standard practice in clinical PET centers for diagnosis of cancer. To make a radiotracer to be widely used, it is necessary to establish a system that can produce high-quality product with the operation easy enough for routine work. We chose TRACERlab MX_{FDG} as the module for [^{18}F]FES synthesis because it is widely used as a simple automatic FDG synthesizer and it has the flexibility in programming and accepts modification to the cassette. However, this module does not have a cooling function, and the cassette has low chemical resistance. In this study, we studied the hydrolysis condition on this module and performed the synthesis without changing the hardware, and also established a formula of high-quality product for clinical use.

2. Materials and methods

2.1. Reagents and equipment

All chemicals were obtained from commercial sources and used without further purification. The precursor (**1**) and the authentic 16α-fluoro-17β-estradiol were purchased from ABX (Radeberg, Germany). The sodium bicarbonate solution and the sodium ascorbate solution used were of pharmaceutical grade. The other reagents and solvents were obtained from Sigma-Aldrich (St. Louis, MO). The synthesis was performed using TRACERlab MX_{FDG} (GE Medical Systems, Milwaukee, WI), which is one of the automatic FDG synthesizers. The high-performance liquid chromatography (HPLC) system was consisted of a pump (LC-10AD, Shimadzu, Kyoto, Japan), a UV detector (SPD-10AVP, Shimadzu) and a NaI(Tl) radioactive detector (RLC-700, Aloka, Tokyo, Japan).

2.2. Process of [^{18}F]FES preparation

The total procedure of [^{18}F]FES preparation consisted of four steps as follows: (a) fluorination, (b) hydrolysis, (c) HPLC purification and (d) formulation (Fig. 1). The automatic synthesis of [^{18}F]FES including Steps a and b were performed on TRACERlab MX_{FDG}. The diagram of the [^{18}F]FES preparation system is shown in Fig. 2.

2.2.1. Synthesis module

TRACERlab MX_{FDG} is a disposable cassette-type module realizing easy modification of chemical process as well as easy operation as routine work without requiring expert knowledge in chemistry. The synthesis program consists of a Microsoft Excel file defining synthesis parameters such as temperature, time, vacuum pressure, three-way cocks and syringe positions.

2.2.2. Preparation of reagents and cassette

The reagents for [^{18}F]FES synthesis were contained in a set of six vials. The content of each vial was as follows: A, 22 mg of Kryptofix 2.2.2 and 7 mg of potassium carbonate mixture in 50% acetonitrile/water (0.6 ml); B, anhydrous acetonitrile (2 ml); C, 2 mg of the precursor in anhydrous acetonitrile (2 ml); D, 0.2 N hydrochloric acid in 90% acetonitrile/water (2 ml); E, 2.8% sodium bicarbonate in water (2 ml); and F, 70% ethanol/water (2 ml). The reagents, except for A, were sealed in standard 10-ml glass vials. The reagent A in 1.2-ml vial was the same to the one used in FDG synthesis.

The cassette was prepared from the FDG synthesis cassette with a little modification keeping aseptic condition (Fig. 2). The alumina N and two C18 Sep-Pak cartridges,

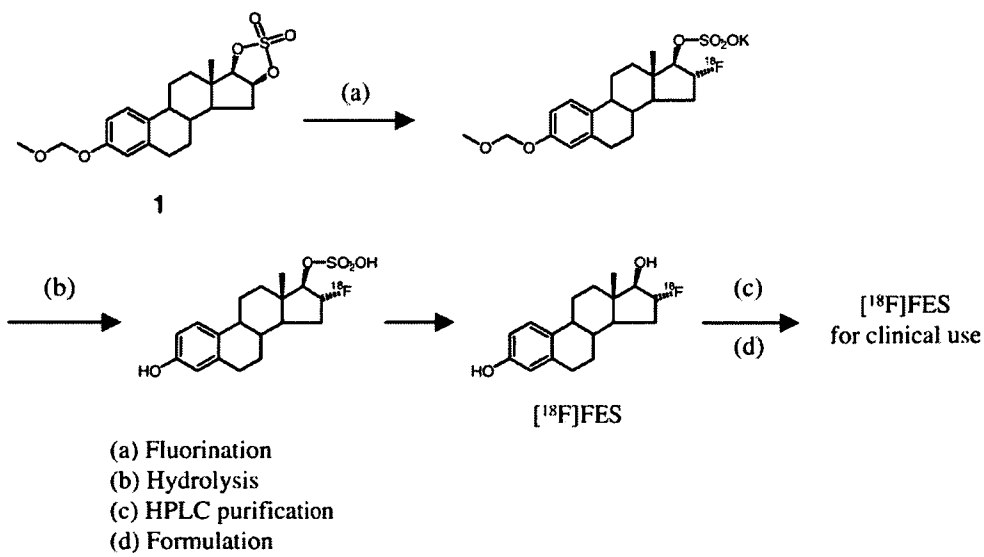

Fig. 1. Scheme of [^{18}F]FES synthesis for clinical use starting from **1**.

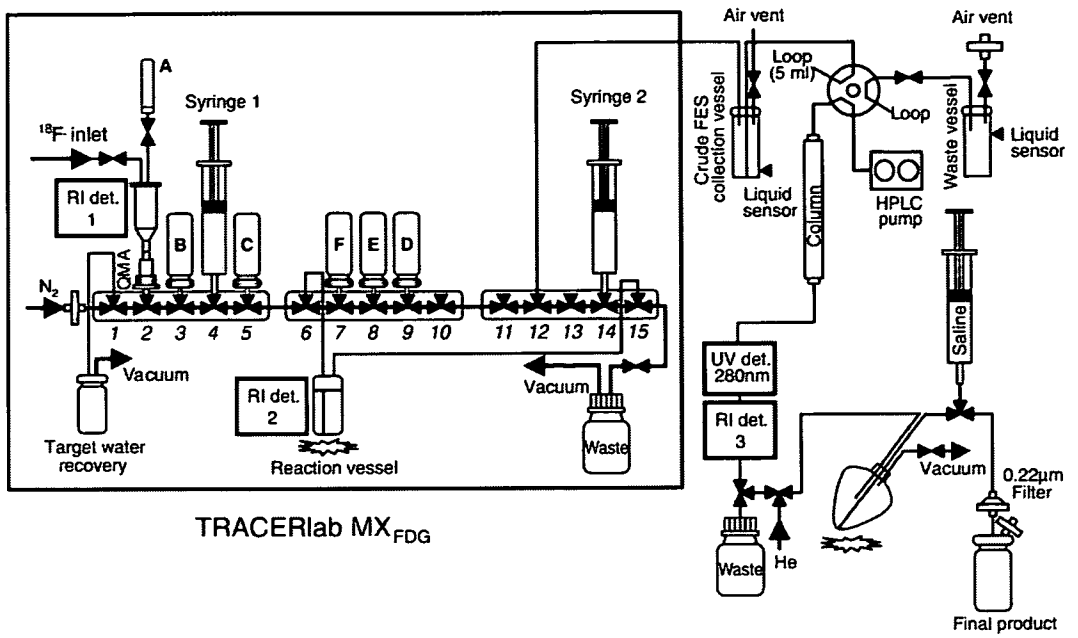

TRACERlab MX$_{FDG}$

Fig. 2. Schematic diagram of the [^{18}F]FES preparation system for clinical use.

unnecessary for [^{18}F]FES synthesis, were removed from the cassette. The water bag connection tube, attached at position 7, was utilized for the central and right manifold connection (positions 10 and 11) after adjustment of the tube length. To add another vial, we moved the male-to-male connector, which had been attached to the C18 Sep-Pak, to position 7 and connected it to an 18G needle. Prior to the synthesis, an activated QMA Sep-Pak light cartridge and two 30-ml polyethylene syringes were jointed to the cassette.

2.2.3. Synthesis of [^{18}F]FES

The synthesis of [^{18}F]FES was modified from the method of Römer et al. [12]. Fluorine-18 was produced by the ^{18}O(p,n)^{18}F reaction using an ultrasmall cyclotron OSCAR (JFE P&S/Oxford, Yokohama, Japan) or RDS eclipse RD/HP (Siemens/CTI, Knoxville, TN) in the PET center of the University of Fukui. The irradiated ^{18}O water, which contained a carrier-free [^{18}F]fluoride, was transferred to the module automatically and passed through the QMA cartridge. The trapped [^{18}F]fluoride on the cartridge was eluted by A into the reaction vessel and dried three times adding small amount of B. The precursor in acetonitrile, C, was added to the reaction vessel for fluorination and heated at 105°C for 10 min. After the fluorination, the solution was transferred to the syringe 1 to release the increased pressure and then returned back to the reaction vessel. The solvent was evaporated to decrease the total volume. To start the hydrolysis, we added D to the reaction vessel and heated it at 95°C for 10 min with the valves closed, which brought a pressurized condition. To stop the hydrolysis, we performed neutralization in syringe 1. The base reagent, E, was transferred to syringe 1 during the hydrolysis, and then the reaction solution was drawn in the same syringe. The mixture was pushed out to the reaction vessel to recover the remaining radioactivity and was drawn again. The radioactive solution was pushed out into the crude FES collection vessel for HPLC purification. The acetonitrile in B (about 1 ml) was used to flush the reaction vessel and the cassette, and added to the crude FES vessel. The reagent F was used for flushing the cassette.

2.2.4. The HPLC purification and the formulation steps

The HPLC purification was performed using a Cosmosil 5C$_{18}$-AR-2 column (20-mm ID×250-mm, Nacalai Tesque, Kyoto, Japan) with acetonitrile/water/ethanol (30:40:30) at a flow rate of 6.0 ml/min. For the HPLC injection, we used a 5-ml sample loop and automatic injector (Rheodyne, Rohnert Park, CA). The desired radioactive fraction was collected in a round-bottom flask containing 0.1 ml of sodium ascorbate (250 mg/ml) in the solvent replacement unit (JFE P&S). The solvent was removed in vacuo and the residue was dissolved in 10 ml of saline, and then passed through a sterile 0.22-μm filter (Millex-GS, Millipore, MA) to a pyrogen-free vial as the final product.

2.3. Evaluation of the products

The radiochemical purity of the product right after the synthesis and in the final product for clinical use was determined by HPLC analysis using a Cosmosil 5C$_{18}$-MS-2 column (4.6-mm ID×150 mm, Nacalai Tesque) with 40% acetonitrile/water at a flow rate of 1.0 ml/min. In this system, [^{18}F]FES was eluted for 8.1 min. To determine the yield of fluorination, we measured the free [^{18}F]fluoride in the crude [^{18}F]FES solution by radio thin-layer chromatography (radio TLC) method. The radio TLC was performed on Merck aluminum backed silica gel 60 plates with chloroform/methanol (4:1). The Rf values of [^{18}F]fluoride

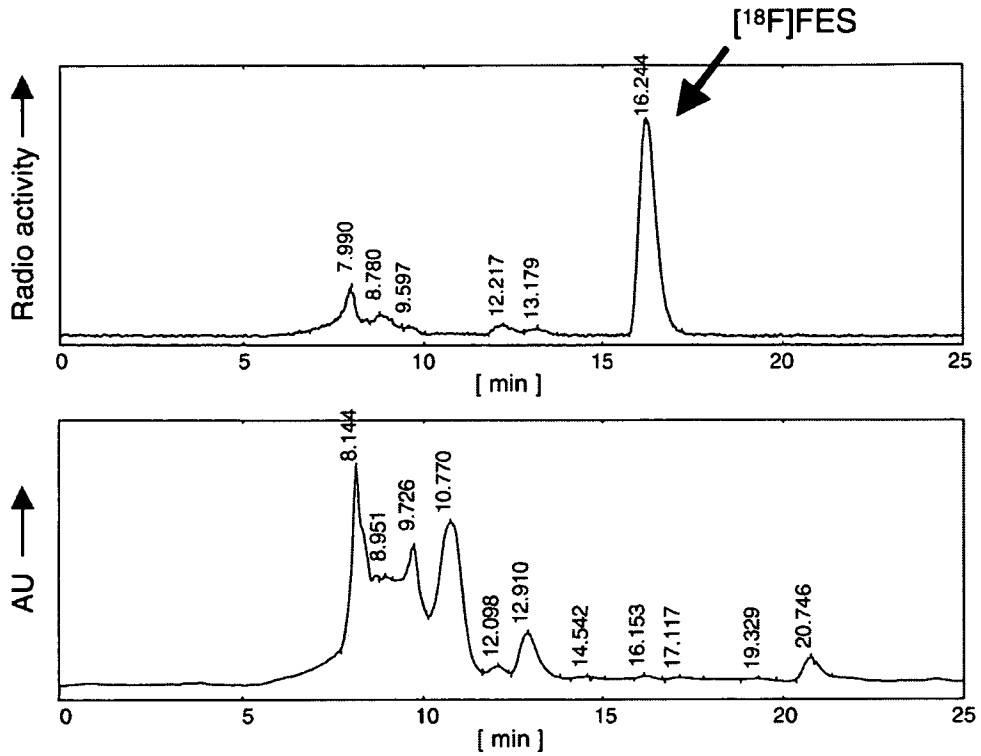

Fig. 3. The chromatograms of the crude [^{18}F]FES at the HPLC purification. Top, radioactivity; bottom, UV absorbance at 280 nm. The retention time of [^{18}F]FES was 16.2 min, which corresponded to the authentic unlabeled 16α-fluoro-17β-estradiol.

and [^{18}F]FES were 0.00 and 0.75, respectively. The other two unknown labeled compounds had Rf values of 0.30 and 0.40.

3. Results and discussion

In this study, we established the optimal procedure for [^{18}F]FES preparation for clinical use through investigating the condition for the synthesis, the purification and the formulation steps. We chose the synthesis method using **1** as the precursor because the reaction can be carried out under mild condition, which is suitable for our module. In addition, **1** is commercially available. The process of [^{18}F]FES synthesis is outlined in Fig. 1. Steps a and b were performed in TRACERlab MX_{FDG}. There were only three points different between the [^{18}F]FES synthesis and the FDG synthesis as follows: the synthesis program, the regents and the cassette layout. The advantage of this method was that the synthesis of [^{18}F]FES and FDG can be performed using the same machine without a change to the hardware.

The fluorination of **1** was performed by the nucleophilic substitution reaction by $K^{18}F$ and accomplished with high yield (89.5±0.8%, n=5). The next hydrolysis step consists of two consecutive reactions. Römer et al. [12] reported two methods of the hydrolysis for their automated module: the pressure hydrolysis method using HCl and the multiple azeotropic evaporation method using hydrochloric acetonitrile. They recommended the latter because it had an advantage of removing the acid and the unreacted [^{18}F]fluoride at the same time. We tried this method, but the radioactivity in the reaction vessel varied between the different runs (40.0±27.3%, n=5). We suspected that the main reason for the inconsistency was decomposition of [^{18}F]FES during the azeotropic evaporation, though it might have depended on the module we used. As it seemed that the decomposition occurred under water-rich condition, we

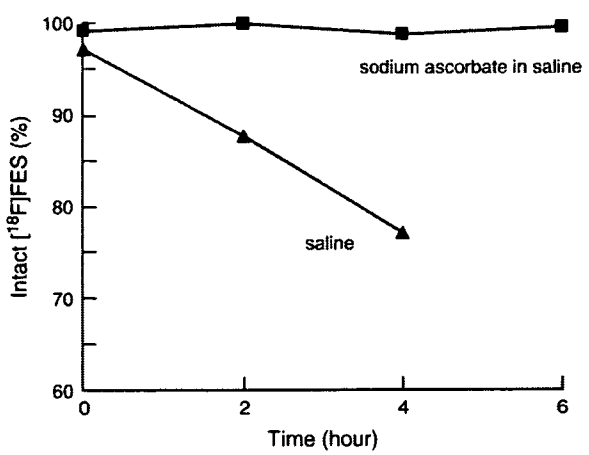

Fig. 4. The stability of [^{18}F]FES in the final product for clinical use. 16α-[^{18}F]fluoro-17β-estradiol was rapidly degraded in saline without sodium ascorbate.

speculated that maintaining acetonitrile/water ratio during the reaction would lead to high and reproducible yield of [^{18}F]FES. In order to keep the acetonitrile component, we carried out the reaction using 90% hydrochloric acetonitrile in closed valve condition. In this condition, [^{18}F]FES was formed within 6 min after the start of hydrolysis at 95°C, and the yield reached the plateau level within another 4 min. Therefore, we decided the reaction time to be 10 min. In this way, most of the radioactivity in the reaction vessel was maintained during the hydrolysis. Fig. 3 shows the chromatogram of the HPLC purification. The retention time of [^{18}F]FES was 16.2 min, which corresponded to that of unlabeled authentic FES. The chromatogram demonstrated that the [^{18}F]FES synthesis was accomplished with a yield of 76.4±1.9% based on the crude [^{18}F]FES solution (n=5). It indicated that the fluorination and the hydrolysis were achieved properly. This method realized sufficiently high and reproducible yields for clinical use as we had intended. The volume of the crude [^{18}F]FES solution was about 3 ml without the reagent F, and the pH of this solution was 8. The purified [^{18}F]FES was stable when the mobile phase of HPLC contained 30% ethanol.

The formula of the final product was also examined. Several researchers provided the final product of [^{18}F]FES as an ethanol/saline solution, probably because of easy preparation from HPLC eluate and high lipophilicity of [^{18}F]FES. However, ethanol causes unacceptable side effects in some patients. Thus, we attempted to prepare the final product as saline solution. However, the radiochemical purity of the product declined rapidly. The percentage of intact [^{18}F]FES was 87% at 2 h (Fig. 4). It indicated that ethanol might be working not only as a solvent but also as a radical scavenger. When sodium ascorbate was added as a radical scavenger instead of ethanol to prevent the decomposition, the radiochemical purity of [^{18}F]FES in saline was over 98% after 6 h. In the filtering process, about 10% of the radioactivity based on input [^{18}F]fluoride was trapped on the membrane filter. Fortunately, the final product through the filter was not trapped much in the final glass vial and the polyethylene syringe used for injection. The radioactivity trapped on the filter could be eluted by 70% ethanol and was confirmed as an intact [^{18}F]FES. Even though our formula causes the decrease of the final product in the filtering process, however, it has the advantage of avoiding the side effects in clinical use. The final product was obtained with a yield of 42.4±3.2% based on input [^{18}F]fluoride (decay corrected, n=5). The specific activity was calculated by the analytical HPLC system (the detection limit was 0.1 μg/ml), and the value was more than 111 GBq/μmol.

The total preparation time was 88.2±6.4 min. The automated synthesis on TRACERlab MX_{FDG} was completed in 50 min. The HPLC purification took 20 min, and another 20 min was required for the formulation process. If the final product was prepared in ethanol/saline solution like in other reports, the ethanol/water solution can be used as the mobile phase in purification, and the following formulation process can be omitted.

4. Conclusion

In this study, we demonstrated that the [^{18}F]FES for clinical use can be prepared with high and reproducible yield using a commercial FDG synthesizer. The merit of our method is that [^{18}F]FES can be easily prepared in a PET institution without a chemist because it does not require expertise in chemistry. Our preparation system enables routine use of [^{18}F]FES in clinical PET centers.

Acknowledgments

We thank Hirokazu Hanawa and Toshinao Nakakoji for operating the CTI cyclotron. Part of this study was supported by the Research and Development Project Aimed at Economic Revitalization from the Ministry of Education, Culture, Sports, Science and Technology (MEXT), Japan; the 21st Centry COE program "Biomedical Imaging Technology Integration Program" from the Japan Society of the Promotion of Science (JSPS); and a grant for the Collaboration of Regional Entities for the Advancement of Technological Excellence (CREATE) from the Japan Science and Technology Agency (JST).

References

[1] Vollenweider-Zerargui L, Barrelet L, Wong Y, Lemarchand-Beraud T, Gomez F. The predictive value of estrogen and progesterone receptors' concentrations on the clinical behavior of breast cancer in women: clinical correlation on 547 patients. Cancer 1986;57:1171–80.

[2] Kiesewetter DO, Kilbourn MR, Landvatter SW, Heiman DF, Katzenellenbogen JA, Welch MJ. Preparation of four fluorine-18 labeled estrogens and their selective uptakes in target tissue of immature rats. J Nucl Med 1984;25:1212–21.

[3] Katzenellenbogen JA, Welch MJ, Dehdashti F. The development of estrogen and progestin radiopharmaceuticals for imaging breast cancer. Anticancer Res 1997;17:1573–6.

[4] Dehdashti F, Flanagan FL, Mortimer JE, Katzenellenbogen JA, Welch MJ, Siegel BA. Positron emission tomographic assessment of "metabolic flare" to predict response of metastatic breast cancer to antiestrogen therapy. Eur J Nucl Med 1999;26:51–6.

[5] Mintun MA, Welch MJ, Siegel BA, Mathias CJ, Brodack JW, McGuire AH, et al. Breast cancer: PET imaging of estrogen receptors. Radiology 1988;169:45–8.

[6] McGuire AH, Dehdashti F, Siegel BA, Lyss AP, Brodack JW, Mathias CJ, et al. Positron tomographic assessment of 16α-[^{18}F]fluoro-17β-estradiol uptake in metastatic breast carcinoma. J Nucl Med 1991;32:1526–31.

[7] Dehdashti F, Mortimer JE, Siegel BA, Griffeth LK, Bonasera TJ, Fusselman MJ, et al. Positron tomographic assessment of estrogen receptors in breast cancer: comparison with FDG-PET and in vitro receptor assays. J Nucl Med 1995;36:1766–74.

[8] Kiesewetter DO, Katzenellenbogen JA, Kilbourn MR, Welch MJ. Synthesis of 16-fluoroestrogens by unusually facile fluoride ion displacement reactions: prospects for the preparation of fluorine-18 labeled estrogens. J Org Chem 1984;49:4900–5.

[9] Brodak JW, Kilbourn MR, Welch MJ, Katzenellenbogen JA. Application of robotics to radiopharmaceutical preparation: controlled synthesis of fluorine-18 16α-fluoroestradiol-17β. J Nucl Med 1986;27:714–21.

[10] Lim JL, Zheng L, Berridge MS, Tewson TJ. The use of 3-methoxymethyl-16β,17β-epiestriol-*O*-cyclic sulfone as the precursor in the synthesis of F-18 16α-fluoroestradiol. Nucl Med Biol 1996;23:911–5.

[11] Lim JL, Berridge MS, Tewson TJ. Preparation of [^{18}F]16α-fluoro-17β-estradiol by selective nucleophilic substitution. J Label Compd Radiopharm 1994;35:176–7.

[12] Römer J, Steinbach J, Kasch H. Studies on the synthesis of 16α-[^{18}F]fluoroestradiol. Appl Radiat Isot 1996;47:395–9.

[13] Römer J, Füchtner F, Steinbach J, Johannsen B. Automated production of 16α-[^{18}F]fluoroestradiol for breast cancer imaging. Nucl Med Biol 1999;26:473–9.

資料(8)

Available online at www.sciencedirect.com

SCIENCE DIRECT

Nuclear Medicine and Biology 33 (2006) 153–158

NUCLEAR MEDICINE — AND — BIOLOGY

www.elsevier.com/locate/nucmedbio

Technical note

New approach to fully automated synthesis of sodium [^{18}F]fluoroacetate — a simple and fast method using a commercial synthesizer

Li-Quan Sun[a], Tetsuya Mori[a], Carmen S. Dence[b], Datta E. Ponde[b], Michael J. Welch[b], Takako Furukawa[a], Yoshiharu Yonekura[a], Yasuhisa Fujibayashi[a,*]

[a]*Biomedical Imaging Research Center, University of Fukui, Yoshida, Fukui 910-1193, Japan*

[b]*Division of Radiological Sciences, Mallinckrodt Institute of Radiology, Washington University School of Medicine, St. Louis, MO 63110, USA*

Received 27 April 2005; received in revised form 6 July 2005; accepted 7 July 2005

Abstract

A simple, rapid and fully automated preparation of sodium [^{18}F]fluoroacetate has been developed by taking advantage of the similarities between the reaction pathways of [^{18}F]fluoroacetate and [^{18}F]-2-fluoro-deoxyglucose (FDG). The automated synthesis of sodium [^{18}F]fluoroacetate was achieved with a commercial [^{18}F]FDG synthesizer, the TRACERlab MX_{FDG}. The method produced the desired compound in a short synthesis time (32 min) and with a high and reproducible radiochemical yield (50.2±4.8%, decay corrected). The radiochemical purity of sodium [^{18}F]fluoroacetate was greater than 99%.

Keywords: Sodium [^{18}F]fluoroacetate; Ethyl [^{18}F]fluoroacetate; Automated synthesis; Commercial synthesizer; PET tracer

1. Introduction

Sodium fluoroacetate (sodium monofluoroacetate, Compound 1080) is well known as a salt with very high mammalian toxicity and is often used as a rodenticide or insecticide [1,2]. This salt is metabolized to fluorocitrate, which cannot be further metabolized to carbon dioxide and blocks the tricarboxylic acid cycle in the body [3,4]. Fluorine-18-labeled sodium fluoroacetate, like [^{11}C]acetate, has been used as a tracer for positron emission tomography (PET) to study myocardial metabolism and cerebral oxidative metabolism [5]. Sodium [^{18}F]fluoroacetate has a longer half-life than [^{11}C]acetate, so it should facilitate diagnostic studies by PET. Recent studies using sodium [^{18}F]fluoroacetate as a tumor imaging agent have been reported, and the results suggested that defluorination of sodium [^{18}F]fluoroacetate was species dependent and occurred in rodents but not in primates [6]. Sodium [^{18}F]fluoroacetate has also been reported to be a useful PET tracer for prostate cancer imaging [7]. It had a high sensitivity for detection of recurrent cancer in prostate [7] and provided higher tumor-to-background ratio than [^{11}C]acetate [6–8].

To realize sodium [^{18}F]fluoroacetate's potential in PET imaging, an automated synthesis carried out in a short period and with a high yield is necessary. In the last decade, several groups reported the preparation of sodium (or potassium) [^{18}F]fluoroacetate [9–12]. However, all of these needed a long synthesis time (>60 min) and provided a low radiochemical yield (<34%). As a result, these methods are unlikely to fulfill the high demand for the radiopharmaceutical if used routinely. We observed that the chemical steps to prepare sodium [^{18}F]fluoroacetate were similar to those used to prepare [^{18}F]-2-fluoro-deoxyglucose (FDG) [13]. Therefore, the instrumentation used in a [^{18}F]FDG synthesis should be able to produce sodium [^{18}F]fluoroacetate. Many automated [^{18}F]FDG synthesizers are commercially available today, each with individual characteristics and advantages. Among them, the TRACERlab MX_{FDG}, designed by GE Medical Systems (Liege, Belgium), was reported to provide a final injection solution of [^{18}F]FDG in a short time (25 min) from the end of bombardment (EOB) with a yield of more than 60% [14]. Therefore, we attempted to utilize

* Corresponding author. Tel.: +81 776 618430; fax: +81 776 61 8170.
E-mail address: yfuji@fmsrsa.fukui-med.ac.jp (Y. Fujibayashi).

0969-8051/$ – see front matter © 2006 Published by Elsevier Inc.
doi:10.1016/j.nucmedbio.2005.07.005

the TRACERlab MX_{FDG} for our fully automatic synthesis of sodium [^{18}F]fluoroacetate. Only minimal modifications were needed to synthesize sodium [^{18}F]fluoroacetate, and these modifications did not affect its intrinsic function as a [^{18}F]FDG synthesizer.

We have established a new automated method to prepare sodium [^{18}F]fluoroacetate using the TRACERlab MX_{FDG}, the complex of $K^{18}F$ and kryptofix 2.2.2 as nucleophile for the fluorination and ethyl *O*-mesyl-glycolate as the precursor.

2. Experiments

2.1. Materials and apparatuses

Ethyl glycolate and methanesulfonyl chloride were obtained from Tokyo Kasei Kogyo (TCI, Tokyo, Japan). Ethyl fluoroacetate and sodium fluoroacetate (as reference standards) were purchased from Wako Industries (Tokyo, Japan). Potassium carbonate, sodium hydroxide, anhydrous magnesium sulfate, hydrochloric acid, anhydrous acetonitrile and methylene chloride were purchased from Sigma-Aldrich Japan K.K. (Tokyo, Japan). Triethylamine and sodium bicarbonate were purchased from Kanto Kagaku (Osaka, Japan). Ethanol [99.5% for high-pressure liquid chromatography (HPLC)] was purchased from Nacalai Tesque (Kyoto, Japan). All reagents and solvents were of the highest purity available and used without further purification unless specifically stated. Sep-Pak QMA Light cartridges, C18 cartridges, Alumina-N cartridges and Oasis HLB Plus cartridges were purchased from Waters (Milford, MA, USA).

Analytical HPLC was performed on a Waters 600E system equipped with Waters 490E programmable multi-wavelength UV detector set at 210 nm and a Bioscan Flow counter (Washington, DC, USA). A reversed phase Hydrosphere C_{18} column (4.6×150 mm, YMC, Kyoto, Japan) was used with C_2H_5OH/H_2O (10/90) as the liquid phase at a flow rate of 1.0 ml/min.

Gas chromatography (GC) was performed using a Shimadzu 14A system equipped with a flame ionization detector. NMR spectra were obtained for solutions in acetonitrile-d_3, using a JEOL's JNM-400 NMR spectrometer (Tokyo, Japan). Radiometric thin-layer chromatography (TLC) was performed in a developing solvent of CH_3CN/H_2O (95/5) with 0.25 mm Silica Gel 60 Sheets F_{254} purchased from Nacalai Tesque. The TLC plates were analyzed using a Bioscan System AR-2000 imaging scanner (Washington, DC, USA).

Millex GS-vented 0.22-μm sterile filters were obtained from Millipore (Bedford, MA, USA). The LAL kits were purchased from Wako Industries. The pH of the solution was measured using a digital pH meter from Nidden (Tokyo, Japan). The disposable kits were purchased from GE Medical Systems. No-carrier-added [^{18}F]fluoride was produced via the ^{18}O (p, n) ^{18}F reaction in a CTI RDS-eclipse cyclotron (11.0 MeV protons) on an enriched ^{18}O water target. The enriched ^{18}O water (atom 97%+) was purchased from Rotem Ind. (Beer Sheva, Israel).

2.2. Modifications to the TRACERlab MX_{FDG}

As the TRACERlab MX_{FDG} was designed solely for the production of [^{18}F]FDG, some modifications were required

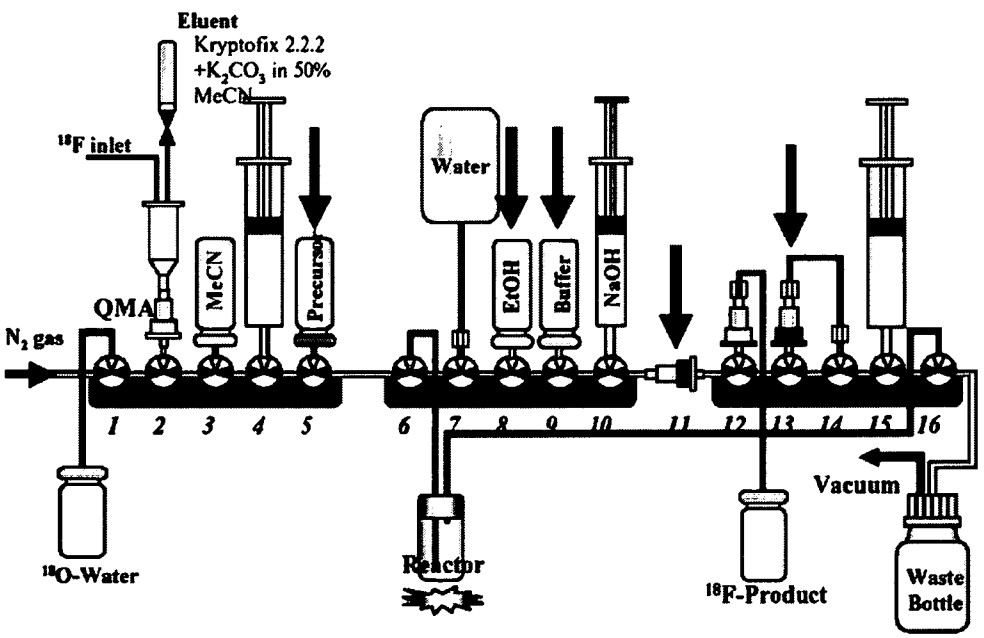

Fig. 1. Schematic diagram of TRACERlab MX_{FDG} for the preparation of [^{18}F]FDG. One Sep-Pak C-18 cartridge was placed at position 11 and another at position 13. The arrows indicate the parts to be replaced for the preparation of sodium [^{18}F]fluoroacetate.

for the preparation of sodium [^{18}F]fluoroacetate. The standard disposable kit and the arrangement of chemical reagents for the preparation of [^{18}F]FDG are shown schematically in Fig. 1. The disposable kit and the arrangement of chemical reagents after the necessary changes for the preparation of sodium [^{18}F]fluoroacetate are shown in Fig. 2. Other parts were not altered except for those documented in Table 1.

A new program file was written to control the automated synthesis of sodium [^{18}F]fluoroacetate. This program is similar to that used for [^{18}F]FDG synthesis, except for changes in the labeling reaction time (from 1 to 5 min), the reaction temperature (from 85°C to 105°C) and the hydrolysis reaction time for the intermediate (from 2 to 5.5 min).

2.3. Preparation of ethyl O-mesyl-glycolate (ethyl α-methanesulfonyl-glycolate)

The synthesis of ethyl *O*-mesyl-glycolate was accomplished following previous methods [9,15] with some modifications. Ethyl glycolate (5.0 g, 48.0 mmol) and methanesulfonyl chloride (6.5 g, 56.7 mmol) were dissolved in 50 ml of methylene chloride in a 200-ml round bottom flask. The solution was cooled to 0°C and triethylamine (5.0 ml, 35.8 mmol) was added dropwise with stirring. After stirring for 80 min at room temperature, the reaction mixture was extracted with ice-cold 1.0 M HCl (70 ml). The organic layer was washed twice with ice-cold water (70 ml) and dried over anhydrous magnesium sulfate. The solution was concentrated by a rotary evaporator and further distilled under reduced pressure. A colorless liquid (6.2 g) was collected at 149°C and 12.0 mm Hg. The liquid was identified as ethyl *O*-mesyl-glycolate with 70.1% yield. ^{1}H NMR (400 MHz, $CDCl_3$, TMS): δ 1.31 (t, 3H, J=7 Hz), 3.22 (s, 3H), 4.25 (q, 2H, J=7 Hz), 4.76 (s, 2H [16]).

Table 1
Content changes performed in the TRACERlab MX_{FDG} from [^{18}F]FDG to sodium [^{18}F]fluoroacetate syntheses

Position	[^{18}F]FDG	[^{18}F]fluoroacetate
3	CH_3CN (7 ml)	CH_3CN (3.5 ml)
5	Mannose triflate	Ethyl *O*-mesyl-glycolate
8	CH_3CH_2OH	$NaHCO_3$ (aq)
9	Buffer	1.0 M HCl (3.0 ml)
10	2.0 M NaOH (1.0 ml)	1.0 M NaOH (2.7 ml)
11	Sep-Pak C18 (X 1)	Oasis HLB Plus (X 1)
13	Sep-Pak C18 (X 1)	Oasis HLB Plus (X 3)

2.4. Preparation of sodium [^{18}F]fluoroacetate

Fluorine-18-labeled sodium fluoroacetate was synthesized by a nucleophilic substitution of the precursor, ethyl *O*-mesyl-glycolate, with potassium [^{18}F]fluoride/kryptofix 2.2.2, followed by a hydrolysis with aqueous sodium hydroxide solution on Oasis HLB Plus cartridges in the TRACERlab MX_{FDG}.

No-carrier-added aqueous [^{18}F]fluoride solution (1.35 ml, 740 MBq to 14.8 GBq) was added to a reserve vessel in the TRACERlab MX_{FDG}, and then the automated synthesis was started. The [^{18}F]fluoride in enriched ^{18}O water was transferred into a Sep-Pak QMA Light cartridge, which had been converted to the CO_3^{2-} form by treatment with

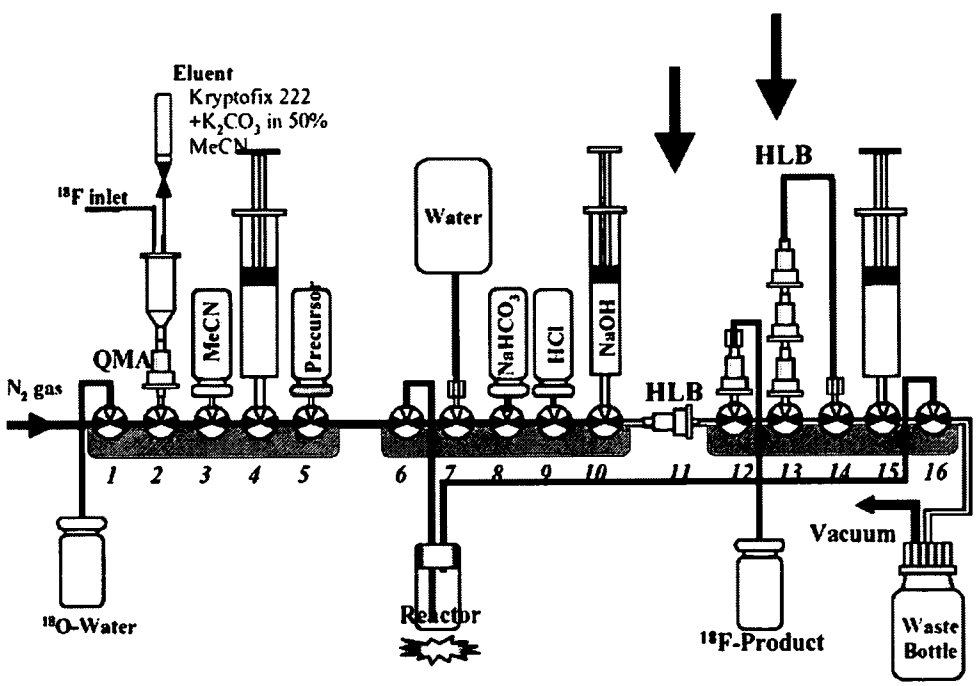

Fig. 2. Schematic diagram of TRACERlab MX_{FDG} for the preparation of sodium [^{18}F]fluoroacetate. Instead of Sep-Pak C-18 cartridges, one Oasis HLB Plus cartridge was placed at position 11 and three at position 13.

an aqueous solution of 0.1 M K_2CO_3. [^{18}F]Fluoride was extracted from the enriched ^{18}O water and trapped on the QMA cartridge, and the enriched ^{18}O water was recovered in the reservoir. A mixed solution of kryptofix 2.2.2 (6.4 mg) in acetonitrile (0.4 ml) and potassium carbonate (0.6 mg) in water (0.3 ml) was employed to elute the trapped [^{18}F]fluoride from the QMA cartridge. The eluate with radioactivity was introduced into the reaction vessel. Water was azeotropically evaporated three times at 95°C under nitrogen gas flow and anhydrous acetonitrile (60 μl×3). After the drying step, 6.2 mg of ethyl *O*-mesyl-glycolate dissolved in 2.2 ml of anhydrous acetonitrile was added to the dried residue in the reaction vessel. The labeling reaction was conducted at 105°C for 5 min in the closed reaction vessel to give rise to ethyl [^{18}F]fluoroacetate. The reaction solution was diluted with 10 ml of distilled water and transferred to Oasis HLB Plus cartridges. The reaction vessel and the cartridges were washed with an additional 30 ml of distilled water to remove the nonreacted [^{18}F]fluoride. The reaction intermediate, ethyl [^{18}F]fluoroacetate, was trapped on the Oasis HLB Plus cartridges. After drying with nitrogen gas flow, 2.7 ml of 1.0 M sodium hydroxide solution was added into the Oasis HLB Plus cartridges, and ethyl [^{18}F]fluoroacetate was base hydrolyzed in the presence of aqueous sodium hydroxide solution. After 5.5 min, the solution in the cartridges was drawn into a 30-ml syringe, and 3 ml of 1.0 M aqueous hydrochloric acid solution was added into the syringe to neutralize the sodium hydroxide. Then, 5 ml of 0.2 M sodium bicarbonate solution was added to adjust the final pH to 5.0–8.0. The solution in the syringe was purified by passage through a Sep-Pak Alumina-N cartridge and filtered through a 0.22-μm sterile filter into a 25-ml sterile vial with 7.4 ml of distilled water. The final solution was analyzed by TLC. The product was also analyzed by HPLC. The total synthesis time was about 32 min.

3. Results and discussion

3.1. Synthesis of ethyl O-mesyl-glycolate

The precursor, ethyl *O*-mesyl-glycolate, was prepared through a nucleophilic substitution reaction. Unlike reported methods [9], instead of using a silica gel column after the reaction, the precursor was directly distilled from the reaction mixture under reduced pressure. This modification simplified the synthesis and avoided introduction of impurities.

3.2. Radiosynthesis of ethyl [^{18}F]fluoroacetate

Ethyl [^{18}F]fluoroacetate is the intermediate produced by the fluorine-18-labeling reaction in the radiosynthesis of sodium [^{18}F]fluoroacetate. During the first attempt to use the complex of K[^{18}F]F and kryptofix 2.2.2 as the nucleophilic agent, we investigated the effects of several reaction conditions, including reaction temperature, reaction time and the amount of the precursor, on the labeling yield.

First, using 60 mg of the precursor dissolved in 2.2 ml of anhydrous acetonitrile, we studied the labeling yield at three temperatures: 75°C, 90°C and 105°C. After the labeling reaction had proceeded for 20 min, the reaction solution was rapidly analyzed by TLC. We conducted three hot runs at each reaction temperature. The labeling efficiencies of ethyl [^{18}F]fluoroacetate were 40.1±8.5%, 57.7±3.6% and 75.4±6.3% at 75°C, 90°C and 105°C, respectively. As a result, a reaction temperature of 105°C was chosen for the radiosynthesis.

Next, we investigated the labeling reaction at four different reaction times (5, 10, 15 and 20 min) in the presence of 60 mg precursor at 105°C. Thin-layer chromatography analyses revealed that the labeling efficiency of the substitution reaction was more than 70% for all four reaction times (Table 2). So a reaction time of 5 min was chosen for the labeling reaction.

Finally, the amount of the precursor needed was evaluated. Using 6.2, 30 and 60 mg of the precursor at 105°C and a reaction time of 5 min, the labeling efficiencies by fluorine-18 were 71.8±8.7% (n=3), 70.5±3.6% (n=3) and 73.4±2.7% (n=3), respectively. As a result, the smallest amount, 6.2 mg, was chosen.

Based on our past experience, the amounts of kryptofix 2.2.2 and potassium carbonate used were 6.4 and 0.6 mg, respectively, in each run in the synthesis. Reduction in the amount of potassium carbonate and kryptofix 2.2.2 did not affect the labeling efficiency.

3.3. Purification and hydrolysis of ethyl [^{18}F]fluoroacetate

As done during the synthesis of [^{18}F]FDG in the TRACERlab MX_{FDG}, we purified the intermediate before its hydrolysis. First, the ethyl [^{18}F]fluoroacetate intermediate was trapped on the reversed phase cartridges. Cartridges containing radioactivity were washed with 30 ml of distilled water to remove nonreacted [^{18}F]fluoride anion, acetonitrile and kryptofix 2.2.2. In the case of [^{18}F]FDG synthesis, two Sep-Pak C18 cartridges were used in this step, and most of the radioactivity was extracted by the cartridges. However, only 3–5% of the radioactivity was trapped when Sep-Pak C18 cartridges were used in the preparation of sodium [^{18}F]fluoroacetate. In previous reports [17,18], Oasis HLB Plus cartridges had higher capacity and selectivity than Sep-Pak C18 cartridges. By using two Oasis HLB Plus

Table 2
The effect of reaction time on the labeling efficiency of ethyl [^{18}F]fluoroacetate

Time (min)	Labeling Efficiency (%)
5	73.4±2.7
10	72.7±6.0
15	70.1±4.8
20	75.4±6.3

The precursor (60 mg) was dissolved in anhydrous CH_3CN (2.2 ml) and heated at 105°C. The labeling reaction was performed three times in each reaction time.